Available online at www.sciencedirect.com
SCIENCE DIRECT®
PERGAMON
International Journal of Heat and Mass Transfer 46 (2003) 4755–4768
International Journal of HEAT and MASS TRANSFER
www.elsevier.com/locate/ijhmt

Species heat and mass transfer in a human upper airway model

Z. Zhang, C. Kleinstreuer *

Department of Mechanical and Aerospace Engineering, North Carolina State University, Raleigh, NC 27695-7910, USA

Received 13 January 2003; received in revised form 2 July 2003

Abstract

Steady 3-D airflow and scalar transport of ultrafine particles, $d_p < 0.1$ μm, and fuel vapors within the human upper airways are simulated and analyzed for laminar as well as locally turbulent flow conditions. Presently, our respiratory system consists of two major segments of a simplified human cast replica, i.e., a representative oral airway from mouth to trachea (Generation 0) and a symmetric four-generation upper bronchial tree model (G0–G3). The simulation has been validated with experimental data in terms of ultrafine particle deposition efficiencies. The present computational results show the following: (1) At low breathing rates ($Q_{in} \approx 15$ l/min), ambient temperature variations ($\Delta T_{max} = 47$ °C) influence the *local* velocity fields and vapor concentrations; however, the total and segmental deposition fractions of fuel vapor in the upper airway are essentially unaffected. (2) The inlet flow rate has a significant effect on vapor deposition, i.e., the higher the flow rate the lower the deposition fraction. (3) The convective heat transfer coefficient averaged over an individual bifurcation unit can be correlated as $Nu = 0.568(RePr)^{0.495}$ $(600 < Re < 6000)$. (4) Two new Sherwood number correlations capture the convective mass transfer for the oral airway and individual bifurcations.

The methodology outlined and physical insight provided can be also applied to other intake configurations, such as engine ports and inlets to air-breathing propulsion systems.

1. Introduction

Inhalation exposure to ultrafine, i.e., nano-scale, airborne particles or various toxic gases and fuel vapors can cause pulmonary and other diseases [1,2]. In contrast, nebulized drug aerosols are now being orally administrated for special treatments [3]. In general, mass transfer due to turbulence and/or Brownian motion is the dominant factor in deposition of ultrafine particles or vapors in the human upper airways [3]. There are relatively few studies on the deposition of such species in the upper human airways, or any other complex intake conduit, primarily because of the difficulty of ultrafine particle generation for experimental measurements and the accurate prediction of its deposition in computational fluid-particle dynamics (CFPD) simulations. In a series of papers, Cheng et al. [4–6] reported their measurements of deposition and mass transfer of ultrafine particles (3.6 nm $< d_p <$ 150 nm) in a human nasal and oral airway cast; Cohen and her colleagues [7,8] reported their experimental work on ultrafine particle and iodine vapor deposition in an upper tracheobronchial airway cast model. Kimbell et al. [9] and Kepler et al. [10] in their numerical analysis part used a commercial software to simulate the gas transport patterns within nasal airways of a rat and a rhesus monkey, respectively. Yu et al. [11,12] simulated the ultrafine particle diffusion in a single bifurcation airway model and a human upper airway model from mouth/nose to the first two generations of the tracheobronchial tree. However, most existing numerical simulations were limited to laminar flow modeling and lacking in detailed validations. Some simulated results appear to deviate from experimental studies; for example, the simulated deposition efficiency in a single bifurcation by Yu et al. [11] seems to be unreasonable because it shows a minor effect of particle size and much higher values for 50 nm particles when compared to similar experimental measurements [7,13]. More importantly, the flow in the human upper airways

* Corresponding author. Tel.: +1-919-515-5216; fax: +1-919-515-7968.
E-mail address: ck@eos.ncsu.edu (C. Kleinstreuer).
URL: http://www.mae.ncsu.edu/research/ck_CFPDlab/index.html

0017-9310/$ - see front matter © 2003 Elsevier Ltd. All rights reserved.
doi:10.1016/S0017-9310(03)00358-2

Nomenclature

A	cross-sectional area
a	thermal diffusion coefficient
c_g	specific heat of the gas
D	tube diameter
$\widetilde{D}$	diffusion coefficient for vapors in air
$\widetilde{D}_p$	diffusion coefficient for ultrafine particles in air
d_p	particle diameter
G	gravitational acceleration
H	enthalpy
h_c	heat transfer coefficient
h_m	mass transfer coefficient
k	turbulence kinetic energy
Le	Lewis number ($a/\widetilde{D}$)
Nu	Nusselt number ($h_c D/\lambda$)
Pr	Prandtl number (v/a)
P	mean static pressure
Q_{in}	inspiratory flow rate
q''	heat flux
Re	Reynolds number (uD/v)
Sc	Schmidt number ($v/\widetilde{D}$)
Sh	Sherwood number ($h_m D/\widetilde{D}$)
s_{ij}	strain-rate tensor
T	temperature
T_{in}	inlet air temperature
T_{ref}	buoyancy reference temperature
u	axial velocity
u_i	mean velocity in tensor notation
u_{in}	mean velocity at the inlet
u_τ	friction velocity ($\sqrt{\tau_w/\rho_w}$)
x_i	position vector in tensor notation
Y	mass fraction
Y_{in}	mass fraction at mouth inlet
y^+	dimensionless distance from wall, sub-layer scaled distance ($u_\tau y/v$)

Greek symbols

β_T	thermal expansion coefficient
ε	turbulence dissipation rate
λ	thermal conductivity of the gas phase
λ_m	mean free path of air
v	kinetic molecular viscosity (μ/ρ)
v_T	kinetic eddy viscosity (μ_T/ρ)
ρ	fluid density
ρ'	temperature dependent density
τ_{ij}	Reynolds stress tensor
ω	pseudo-vorticity, dissipation per unit turbulence-kinetic-energy

under medium and high-level breathing conditions (say, $Q_{in} = 30$ and 60 l/min, i.e., $Re_{trachea} \approx 3000$ and 6000) may transit from laminar to turbulent after the constriction of the larynx and then relaminarizes in the first several generations [14]. Hence, there is a need for systematical studies of mass transfer in the human upper airways under different breathing conditions in which turbulent dispersion and Brownian motion are combined.

Accompanied by species mass transfer is usually the conditioning process of the inspired air, which may affect nano-particle or vapor transport and deposition. There have been a number of reports published attempting to quantify heat transfer in the human airways. For example, Johnson et al. [15] obtained a convective heat transfer coefficient, h_c, averaged over three bronchial generations for the measured in vivo airway temperatures of several anesthetized, intubated and mechanically respired mongrel dogs. However, the correlation extrapolated from the canine measurements should be carefully examined before it is interpreted for humans. Nuckols [16] carried out a series of convective heat transfer experiments with a cast replica of human upper airways extending from the mouth and nose to the trachea as well as with a mechanical bronchial airway model representing generations G0–G2 after Weibel [17]. Considering inspiration only, he expressed his results in terms of Nusselt numbers averaged over the entire cast from mouth to trachea and the bronchial airway model as follows

For the mouth-to-trachea section:

$$Nu = 0.035(RePr)^{0.804} \tag{1}$$

For the bronchial generations:

$$Nu = 0.0777(RePr)^{0.726} \tag{2}$$

Both Johnson et al. [15] and Nuckols [16] did not derive inspiratory convective heat transfer coefficients for each individual generation of the upper bronchial airways. In summary, past mathematical models and numerical simulations focused only on 1-D and 2-D temperature distributions in the human airways [18–21, among others]. Three-dimensional, coupled heat transfer and airflow in the human respiratory system have not been investigated.

In this paper, considering a human upper airway model from mouth to the first four generation of the tracheobronchial tree, steady 3-D airflow as well as heat and mass transfer are simulated and analyzed for different inspiratory laminar/turbulent flow rates. Focusing on highly toxic vapor from JP-8 fuel, as used worldwide

in military aircrafts, local mass fraction distributions and wall depositions in the upper airway model are investigated as well. Finally, the convective heat and mass transfer coefficients in the human upper airways are calculated and expressed in terms of dimensionless groups. The methodology outlined and physical insight provided can be also applied to other complex intake configurations, such as engine ports and inlet conduits of air-breathing propulsion systems.

2. Theory

2.1. Upper airway geometry

The present upper airway model as shown in Fig. 1 consists of two parts: an oral airway model, including oral cavity, pharynx, larynx and trachea, and a symmetric triple bifurcation lung airway model representing generations G0 (trachea)–G3 after Weibel [17]. The dimensions of the oral airway model were adapted from a human cast as reported by Cheng et al. [4]. The dimensions of the four-generation airway model are similar to those given by Weibel for adults with a lung volume of 3500 ml. The airway conduit is assumed to be smooth and rigid. The effects of cartilaginous rings [22] which may appear in the upper airways have not been considered in the present analysis.

2.2. Governing equations

Airflow and heat transfer: In order to capture the air flow structures in the laminar-to-turbulent flow regimes, i.e., $300 < Re_{\text{local}} < 10^4$ for the present airway configuration and inhalation rates, the low-Reynolds-number (LRN) k–ω model of Wilcox [23] was selected and adapted which has been demonstrated to be appropriate for such internal flows [14]. In general, the transport equations in tensor notation, implying the double-index summation convention, read [23]:

Continuity equation:

$$\frac{\partial u_i}{\partial x_i} = 0 \tag{3}$$

Momentum equation:

$$\frac{\partial u_i}{\partial t} + u_j \frac{\partial u_i}{\partial x_j} = -\frac{1}{\rho}\frac{\partial p}{\partial x_i} + \frac{\partial}{\partial x_j}\left[(\nu + \nu_{\mathrm{T}})\left(\frac{\partial u_i}{\partial x_j} + \frac{\partial u_j}{\partial x_i}\right)\right] + \frac{f_j}{\rho} \tag{4}$$

Turbulent kinetic energy (k) equation:

$$\frac{\partial k}{\partial t} + u_j \frac{\partial k}{\partial x_j} = \tau_{ij}\frac{\partial u_i}{\partial x_j} - \beta^* k\omega + \frac{\partial}{\partial x_j}\left[(\nu + \sigma_k \nu_{\mathrm{T}})\frac{\partial k}{\partial x_j}\right] \tag{5}$$

Pseudo-vorticity (ω) equation:

$$\frac{\partial \omega}{\partial t} + u_j \frac{\partial \omega}{\partial x_j} = \alpha\frac{\omega}{k}\tau_{ij}\frac{\partial u_i}{\partial x_j} - \beta\omega^2 + \frac{\partial}{\partial x_j}\left[(\nu + \sigma_\omega \nu_{\mathrm{T}})\frac{\partial \omega}{\partial x_j}\right] \tag{6}$$

where the turbulent viscosity is given as $\nu_{\mathrm{T}} = c_\mu f_\mu k/\omega$, and the function f_μ is defined as $f_\mu = \exp[-3.4/(1 + R_{\mathrm{T}}/50)^2]$ with $R_{\mathrm{T}} = \rho k/(\mu\omega)$. The other coefficients in the above equations are:

$$C_\mu = 0.09, \quad \alpha = 0.555, \quad \beta = 0.8333, \quad \beta^* = 1, \quad \sigma_k = \sigma_\omega = 0.5. \tag{7a–f}$$

The Boussinesq model is employed for the calculation of the buoyancy force, $f_j = \rho' g$, where the bulk density is

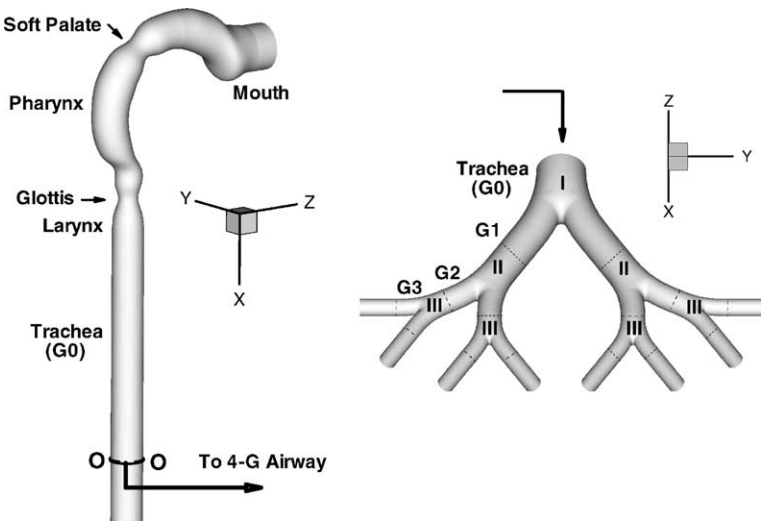

Fig. 1. 3-D views of the oral airway model and bifurcation airway model (generations G0–G3). I—first bifurcation, II—second bifurcation, III—third bifurcation (the dashed lines indicate the segmental boundaries).

not dependent on temperature, pressure or additional variables. The local density variation is defined as

$$\rho' = \rho[1 - \beta_T(T - T_{ref})] \tag{8}$$

For the temperature distribution calculations, the energy equation can be written as [24]

$$\frac{\partial(\rho T)}{\partial t} + \frac{\partial}{\partial x_j}(\rho u_j T) = \frac{\partial}{\partial x_j}\left[\left(\frac{\lambda}{c_g} + \frac{\rho \nu_T}{\sigma_T}\right)\frac{\partial T}{\partial x_j}\right] \tag{9}$$

where σ_T is turbulent Prandtl number for temperature taken as 0.9.

The associated boundary conditions include uniform velocity and temperature profiles prescribed at the mouth inlet, and zero pressure at the outlets. Long exit tube that extends about nine tube diameters from the end of the trachea was used in the oral airway model to eliminate the influence of the zero-pressure assumption at the outlet. However, because the actual length from the glottis to the first carina in the trachea is about 14 cm, the mean-velocity field, turbulence quantities, temperature and mass fraction distributions in the trachea with about 11 cm from the glottis, were adjusted as the inlet conditions of the bifurcating airway segment (i.e., generations G0–G3) (see Fig. 1). The inlet tube length of the bifurcation airway model is about 3 cm.

At the mouth inlet, the values for k and ω were assigned using the following empirical relation [14,25]:

$$k = 1.5(I \times u_{in})^2 \quad \text{and} \quad \omega = k^{0.5}/(0.3D) \tag{10}$$

where I is the turbulence intensity usually taken as 0.037. The thermal boundary condition for air at the air–wall interface is assumed to be at the alveolar condition, and that the airway tissue can provide all the required heat regardless of the amount extracted by the inspired air due to its rich blood supply [26], i.e., $T_{wall} = 310$ K. Two ambient conditions were considered in this paper. One is under "cold weather" condition, i.e., the inlet air temperature $T_{in} = 263$ K, and the other is for warm weather, i.e., $T_{in} = 310$ K, which is equivalent to isothermal flow.

Mass transfer of vapor or ultrafine particles: The convection mass transfer equation of ultrafine particles or (JP-8) fuel vapor whose dominant radial transfer mechanisms are Brownian motion and turbulent dispersion can be given as

$$\frac{\partial Y}{\partial t} + \frac{\partial}{\partial x_j}(u_j Y) = \frac{\partial}{\partial x_j}\left[\left(\widetilde{D} + \frac{\nu_T}{\sigma_Y}\right)\frac{\partial Y}{\partial x_j}\right] \tag{11}$$

where $\sigma_Y = 0.9$ is the turbulence Prandtl number for Y. JP-8 fuel is a multi-component mixture which consists mainly of C8–C16 paraffinic hydrocarbons with other hydrocarbons and additives also present; however, the diffusivity in air does not vary significantly from compound to compound [27]. Thus, a conservative assumption would be to set $\widetilde{D} = 0.05$ cm^2/s for all fractions of JP-8 jet fuel at $T = 293$ K with little loss in accuracy [27]. The effect of temperature change on diffusivity is expressed by the following semiempirical correlation [24]:

$$\widetilde{D}(T)/\widetilde{D}(T = 293\ \text{K}) = (T/293)^{1.75} \tag{12}$$

The aerosol diffusion coefficient is calculated as follows [3,6]:

$$\widetilde{D}_p = (k_B T C_{slip})/(3\pi\mu d_p) \tag{13}$$

where k_B is the Boltzmann constant (1.38×10^{-23} J K^{-1}); and C_{slip} is the Cunningham slip correction factor:

$$C_{slip} = 1 + \frac{2\lambda_m}{d_p}\left[1.142 + 0.058\exp\left(-0.999\frac{d_p}{2\lambda_m}\right)\right] \tag{14}$$

Assuming that the airway wall is a perfect sink for aerosols or vapors upon touch, the boundary condition on the wall is $Y_w = 0$. This assumption is reasonable for fast gas-wall reaction kinetics [28], or vapors of high solubility and reactivity, and also suitable for estimating the maximum deposition of toxic vapor in the airways.

3. Numerical method

The numerical solutions of the continuity and momentum equations as well as the k, ω, heat and mass transfer equations were carried out with a user-enhanced commercial finite-volume based program, i.e., CFX4.4 from AEA Technology [25]. The numerical program uses a structured, multiblock, body-fitted coordinate discretization scheme. In the present simulation, the PISO algorithm with under-relaxation was employed to solve the flow equations. A higher-order upwind (HUW) differencing scheme, which is second-order accurate in space, was used to model the advective terms of the transport equations. The sets of linearized and discretized equations for all variables were solved using the Block Stone's method.

The computational mesh was generated with CFX Build4. The near-wall region required a very dense mesh. Specifically, the thickness of the near-wall cells was chosen to fully contain the viscous sub-layers and to resolve any geometric features present there. As a requirement of low-Reynolds-number turbulence modeling, the first grid point above the wall was given a value of $y^+ \leqslant 1$, and this criterion is strictly maintained for all computations. The mesh topology was determined by refining the mesh until grid independence of the solution of flow, temperature and mass fraction fields was achieved. The final mesh contains about 420,000 and 670,000 cells for the oral airway and four-generation airway model, respectively. The computations were performed on an SGI Origin 2400 workstation with

32GB RAM and multiple 450 MHz CPUs. The steady-state solution of the flow field was assumed to be converged when the dimensionless mass residual, (total mass residual)/(mass flow rate) $< 10^{-3}$. The convergence of other variables was monitored as well. Typical run time for the fluid flow, energy and mass transfer simulations on eight processors with parallel algorithm was approximately 24 h for the oral airway model and 8 h for the four-generation model.

4. Model validation

The present computational fluid-particle dynamics model has been validated with various experimental data sets for steady and transient laminar flows in bifurcations [29,30] and for laminar, transitional and turbulent flows in tubes with local obstructions [14,31]. All our previous contributions dealt with fine, i.e., micro-size, particles for which a spherical form of Newton's second law of motion was employed. The validation results of mass transfer modeling with turbulent flow are given in Fig. 2. Ultrafine particle deposition fractions in the oral airway model obtained from the solution of the mass transfer equation (11) are compared in Fig. 2 with experimental data of Cheng et al. [5] for an inhalation rate of $Q_{in} = 30$ l/min. It can be seen that the simulated results agree well in terms of values and data trend with the experimental findings, considering the experimental uncertainties. Smaller particle diameters indicate higher diffusivities, and hence enhanced particle deposition by diffusion (Fig. 2).

In summary, the good agreements between experimental observations and theoretical predictions instill confidence that the present computer simulation model is sufficiently accurate to analyze laminar-to-turbulent fluid flow as well as heat and mass transfer in three-dimensional oral and bifurcating airways.

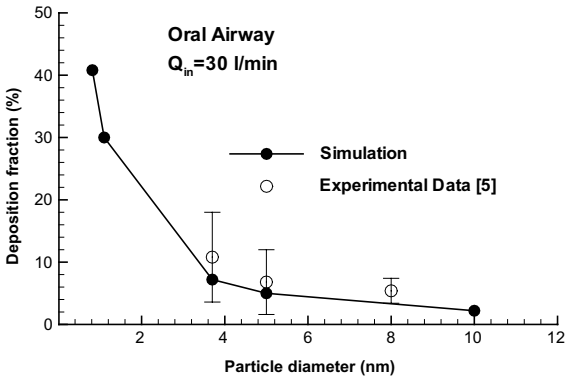

Fig. 2. Comparison of simulated ultrafine particle deposition fractions in the oral airway model with the experimental data of Cheng et al. [5].

5. Results and discussion

Some selected results from our simulations for different inspiratory flow rates and inlet air temperatures are given below. The corresponding Reynolds numbers in the trachea for all simulation cases are listed in Table 1. It should be noted that the web site, listed with the "corresponding author" information contains Figs. 3–7 in color as well as movie clips of airflow, micro-particle transport and vapor dispersion in a human upper airway model.

5.1. Airflow structures

Fig. 3a shows mean velocity profiles in the $y = 0$ plane of the oral airway model with inlet air temperatures of $T_{in} = 263$ and 310 K and an inspiratory flow rate of $Q_{in} = 15$ l/min, i.e., low-level breathing. The selected cross-sectional views in Fig. 3b and c display the axial velocity contours as well as secondary velocity vectors. Clearly, skewed velocity profiles generated by the centrifugal force can be observed in the curved portion from the oral cavity to the pharynx/larynx. Moreover, a central asymmetric jet and a recirculation zone are created in the laryngeal region because of the restriction of the (assumed stationary) vocal folds. The secondary motion is set up when the flow turns a bend from the mouth to the pharynx because of the centrifugally induced pressure gradient [31]. In comparing the velocity profiles with $Q_{in} = 15$ l/min under the cold weather condition with those shown for isothermal flow with $T_{in} = 310$ K, considerable thermal effects can be seen after the glottis. Specifically, strongly buoyant flow near the wall enhances fluid mixing so that the length of the recirculating zone as well as the laryngeal jet zone decreases. At the same time, secondary flows become very weak and a high axial velocity zone is generated in the tube center.

The inspiratory flow rates may influence the flow fields in the oral airway model. For medium-level breathing (say, $Q_{in} = 30$ l/min), the turbulent fluctuations are weak in the oral cavity; but, it becomes strong after the constriction of soft palate and rises rapidly after the glottis, eventually decaying more slowly while approaching an asymptotic level. With further

Table 1
Reynolds numbers in the trachea ($Re_{trachea}$) for different simulated cases

Inlet air temperature (K)	263			310		
Inspiratory flow rate (l/min)	15	30	60	15	30	60
Reynolds number in the trachea	1600	3200	6400	1400	2800	5600

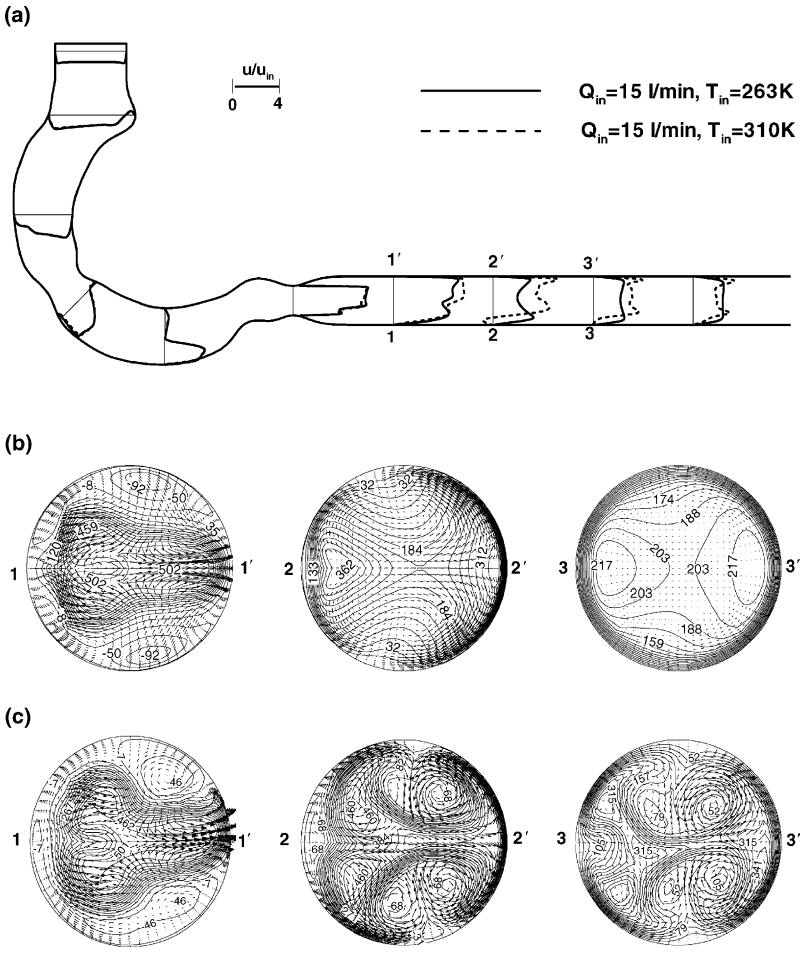

Fig. 3. Velocity distributions in the oral airway model: (a) velocity profiles at side-plane ($y = 0$ plane); (b) axial velocity contours (magnitudes in cm/s) and secondary velocity vectors at different cross-sections at $Q_{in} = 15$ l/min and $T_{in} = 263$ K; and (c) axial velocity contours (magnitudes in cm/s) and secondary velocity vectors at different cross-sections at $Q_{in} = 15$ l/min and $T_{in} = 310$ K.

redistribution of the kinetic energy of the flow over most of the cross-section accompanied by the onset of turbulence, the velocity profiles become more blunt from the left to the right wall, and the maximum velocity zone moves to the anterior wall at the cross-section six diameters from the glottis [31]. The flow features for the strong breathing mode ($Q_{in} = 60$ l/min) resemble those for $Q_{in} = 30$ l/min. However, thermal effects tend to be minor for the high flow rate cases (i.e., $Q_{in} = 30$ and 60 l/min), which are not included.

Fig. 4 depicts mid-plane velocity fields in generations G0–G3 for different inspiratory flow rates with an inlet air temperature of $T_{in} = 263$ K. The air stream with a slightly asymmetric inlet velocity profile splits at the first flow divider and a new boundary layer is generated at the inner wall of the daughter tube. The velocity profiles are naturally skewed in each daughter tube, and hence, each daughter tube, or generation, experiences a different flow rate. The detailed description of airflow structures in the tubular bifurcations may be found in our previous papers [29,30]. Because of the low turbulence intensity in bifurcating tubes even for relatively high inlet flow rate cases, the influence of inlet flow rates on the velocity profiles is not pronounced. The thermal effects are also minor for all three inhalation flow rates due to the warming up of the air when passing through the oral airway.

5.2. Temperature distributions

Fig. 5a and b present the temperature distributions in the human upper airways in terms of non-dimensional temperature profiles, i.e., $\theta = (T - T_{wall})/(T_{in} - T_{wall})$. Clearly, a higher temperature is observed near flow separation as well as stagnation and low-velocity zones, because the convection heat transfer is relatively low in

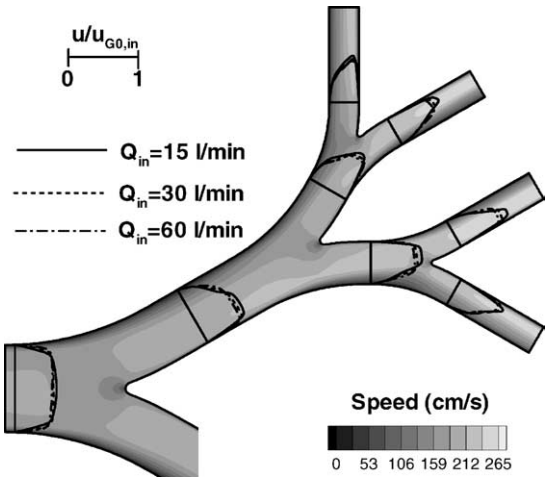

Fig. 4. Velocity profiles in the bifurcation airway model ($z = 0$ plane) with $T_{in} = 263$ K. The speed contour is for the case of $Q_{in} = 30$ l/min and $T_{in} = 263$ K.

these regions and heat cannot be dissipated easily. In the oral airway, the temperature fields influenced by the free airstreams are complicated in the mouth-to-pharynx and larynx regions. But in the trachea, the temperature distribution tends to be more uniform due to the strong energy mixing, driven by the upstream secondary flows (Fig. 5a). Moreover, the air warms up more rapidly with a low inspiratory flow rate ($Q_{in} = 15$ l/min) since the low-speed flow implies a high residence time for the air in the airways with $T_{wall} = 310$ K. In the bifurcating airways G0–G3 (Fig. 5b), asymmetric and skewed temperature distributions exist in different tubes caused by the corresponding velocity fields. Again, the lower the inhalation flow rate, the faster the air warms up, almost attaining the body temperature at the outlets of G3.

5.3. Distributions of mass fractions

Focusing on (JP-8) fuel vapors, the mass fraction contours in the oral airway and airway segment G0–G3 for different inhalation rates are displayed in Figs. 6 and 7. A uniform vapor concentration condition was assumed at the mouth inlet. Similar to the temperature distribution, areas of low velocities are associated with low concentrations due to the low convective mass

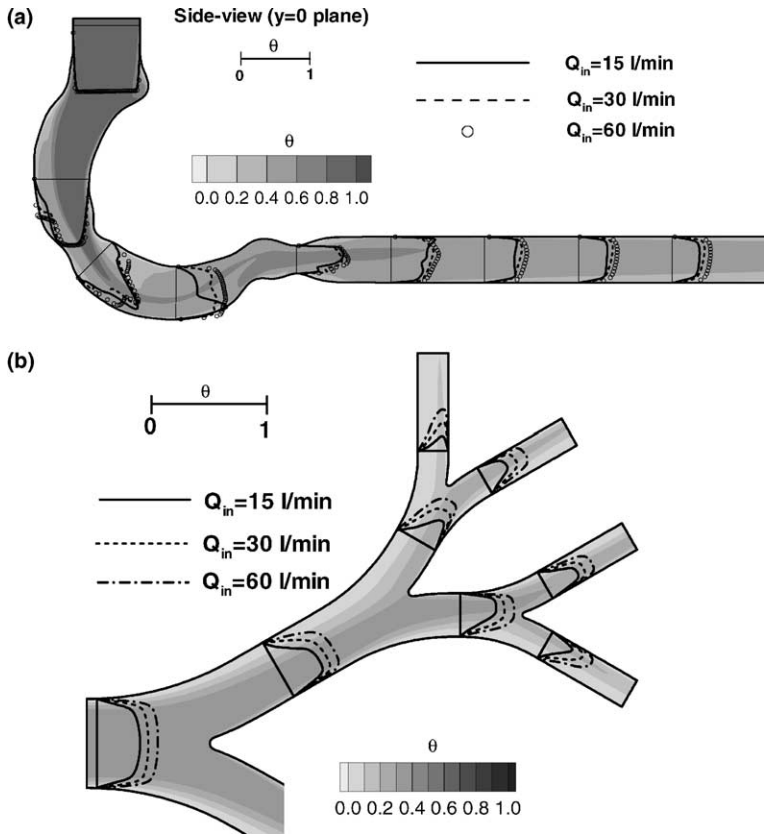

Fig. 5. Non-dimensional temperature profiles in: (a) the oral airway model ($y = 0$ plane); and (b) bifurcation airway model ($z = 0$ plane). Temperature contours are shown for $Q_{in} = 30$ l/min and $T_{in} = 263$ K.

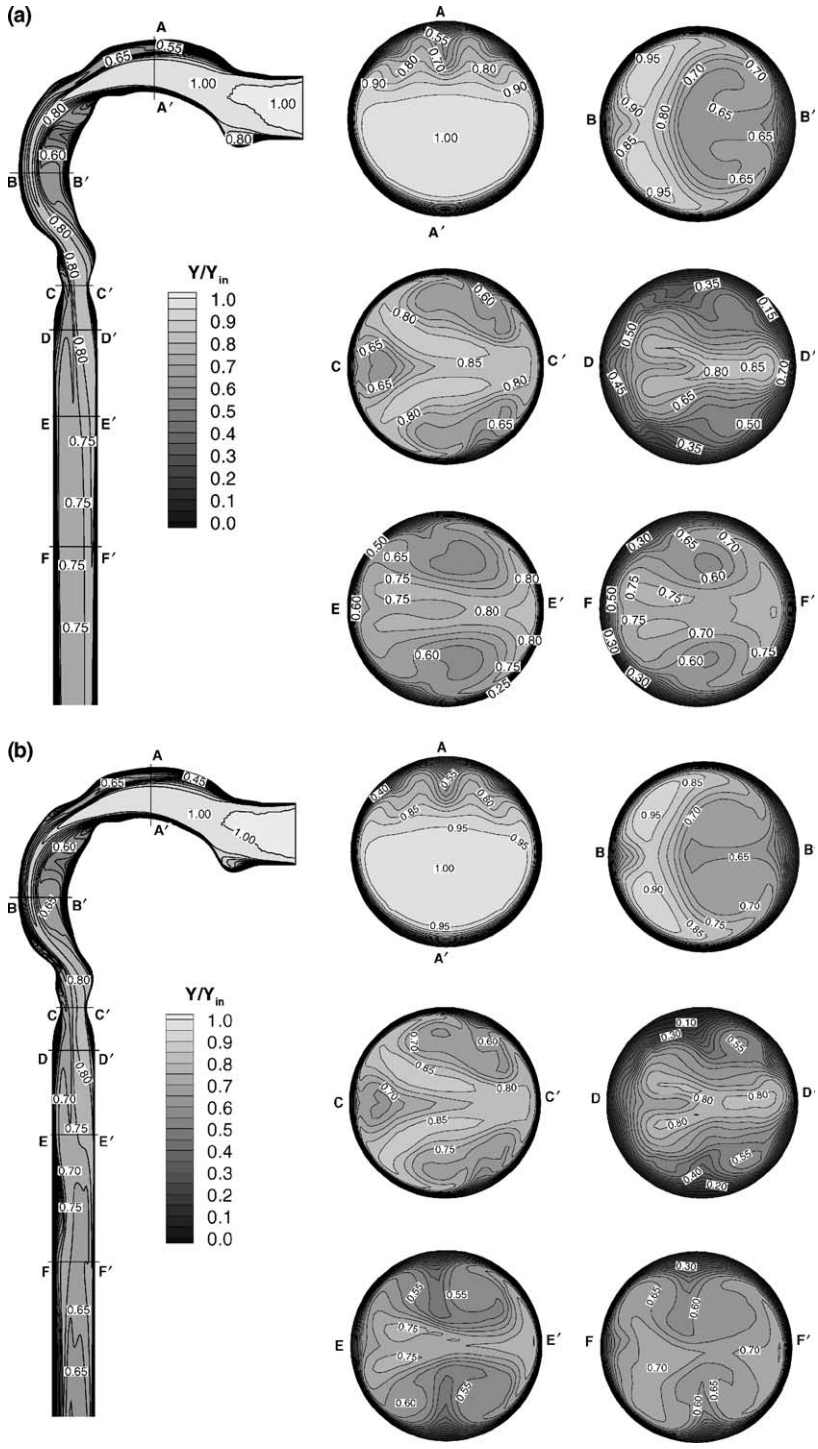

Fig. 6. Concentration contours of JP-8 fuel vapors in the oral airway model at: (a) $Q_{in} = 15$ l/min and $T_{in} = 263$ K; (b) $Q_{in} = 15$ l/min and $T_{in} = 310$ K; and (c) $Q_{in} = 60$ l/min and $T_{in} = 263$ K. The left panels exhibit side-plane ($y = 0$ plane) concentration contours, while the right panels show the concentration distributions at different cross-sectional planes.

transfer. The local concentration gradient near the wall indicates the vapor deposition rate at that site. Thus, the local deposition rate tends to be high at the oral cavity and becomes low in the trachea due to the vapor redis-

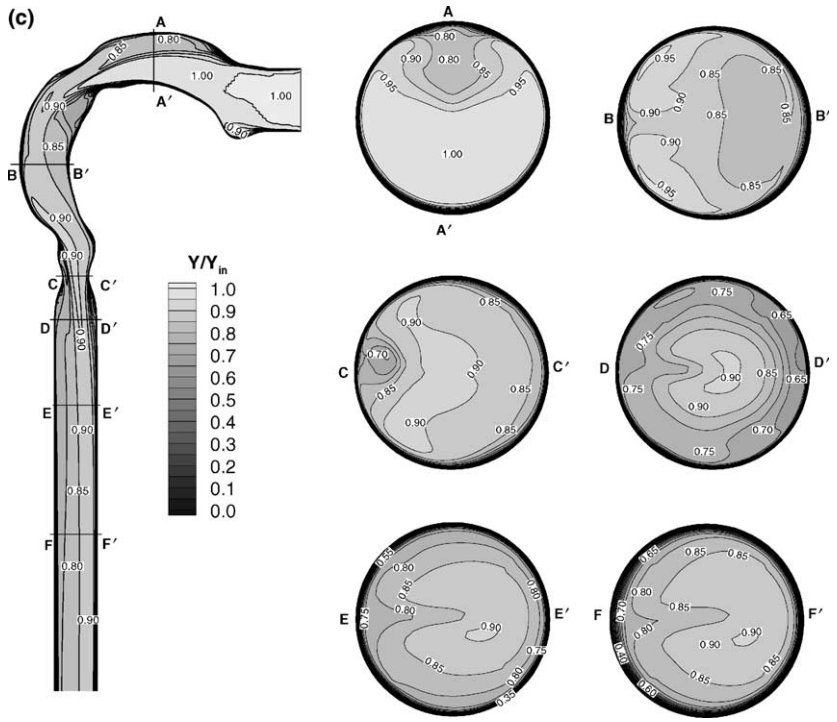

Fig. 6 (*continued*)

tribution over the cross-sections driven by secondary and reverse flows. The vapor field in the trachea for $Q_{in} = 15$ l/min cannot be mixed as rapidly as the heat where the temperature distributions tend to be uniform at E–E' and F–F'. This may be attributed to the relatively high Lewis number for JP-8 vapor ($Le \cong 4$).

Comparing Fig. 6a with Fig. 6b, some thermal effects on concentration distribution can be observed after the glottis for this low inspiratory flow rate case. Specifically, the concentration contours at sections E–E' and F–F' are somewhat different with different inlet air temperatures and the concentration at the tube center of cross-section F–F' is a little higher for the lower inlet temperature case. At the medium and high inspiratory flow rate cases (i.e., $Q_{in} = 30$ and 60 l/min), the concentration in the trachea tends to be more uniform with the onset of turbulence (see Fig. 6c for $Q_{in} = 60$ l/min case). The thermal effects tend to be negligible for medium and high-flow-rate cases ($Q_{in} = 30$ and 60 l/min).

In the airway segment G0–G3 (Fig. 7), the mass transfer patterns are also strongly affected by the skewed and asymmetric velocity profiles, which indicate different vapor depositions in different airway tubes.

5.4. Deposition of fuel vapor

Evaluation of injuries from inhalation exposure to toxic vapors or particles requires detailed knowledge of the inhaled amount and distribution in human airways. The inhaled dose of vapors or ultrafine particles is described by the deposition fraction (DF), which is defined as

$$DF = 1 - \left(\sum_{i=1}^{n} \int u_i Y_i \, dA_i \right) \Big/ \left(\int u_0 Y_0 \, dA_0 \right) \qquad (15)$$

where A is the tube cross-sectional area, and u is the axial velocity. The subscripts "0" and "i" denote the properties at the inlet and the ith daughter tube of a selected generation, respectively. In the oral airway model, the "i" denotes the trachea and $n = 1$. The deposition fractions of JP-8 fuel vapor in the upper airways under different inhalation conditions are shown in Fig. 8a–c. It can be seen from Fig. 8a that higher vapor deposition corresponds to larger inlet air temperatures, especially for the high inhalation flow rate case. This can be attributed to the relatively large diffusion coefficient at relatively high temperatures (see Eq. (12)). Generally speaking, the deposition fraction is weakly affected by the inlet air temperature for both low and high inspiratory flow rates. In other words, the thermal effects could be negligible when calculating the total or segmental deposition fraction of vapors or ultrafine particles in the upper airways. The flow rate also shows a significant effect on the deposition of vapor (cf. Fig. 8b and c). The higher the flow rate, the lower is the deposition fraction. This may be because of the longer

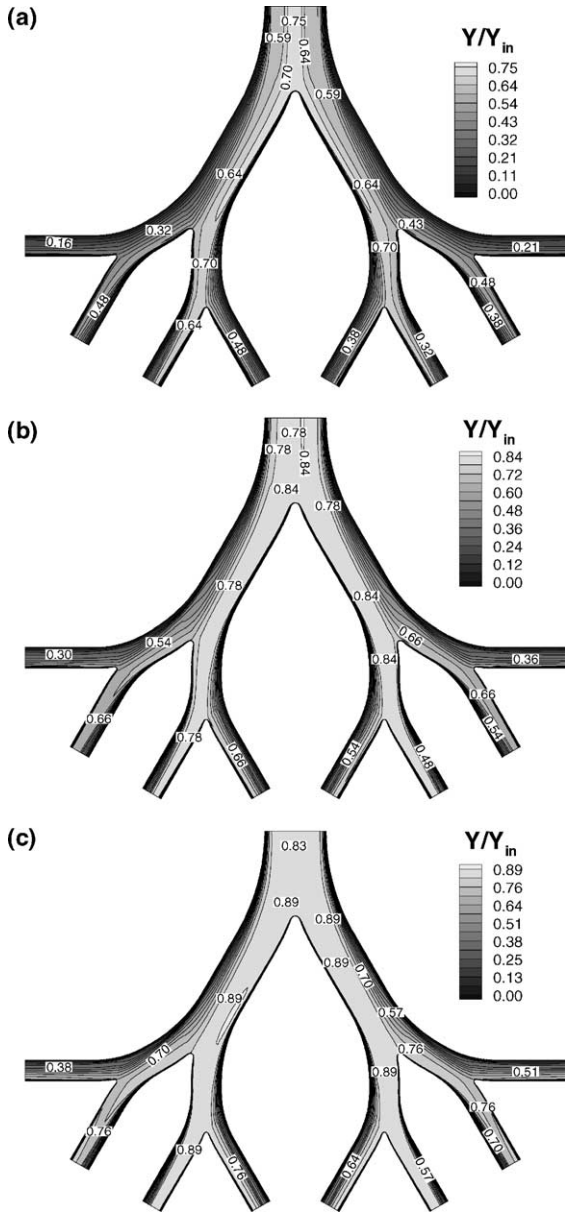

Fig. 7. Concentration contours of JP-8 fuel vapor in the bifurcation airway model ($z = 0$ plane) at: (a) $Q_{in} = 15$ l/min and $T_{in} = 263$ K; (b) $Q_{in} = 30$ l/min and $T_{in} = 263$ K; and (c) $Q_{in} = 60$ l/min and $T_{in} = 263$ K.

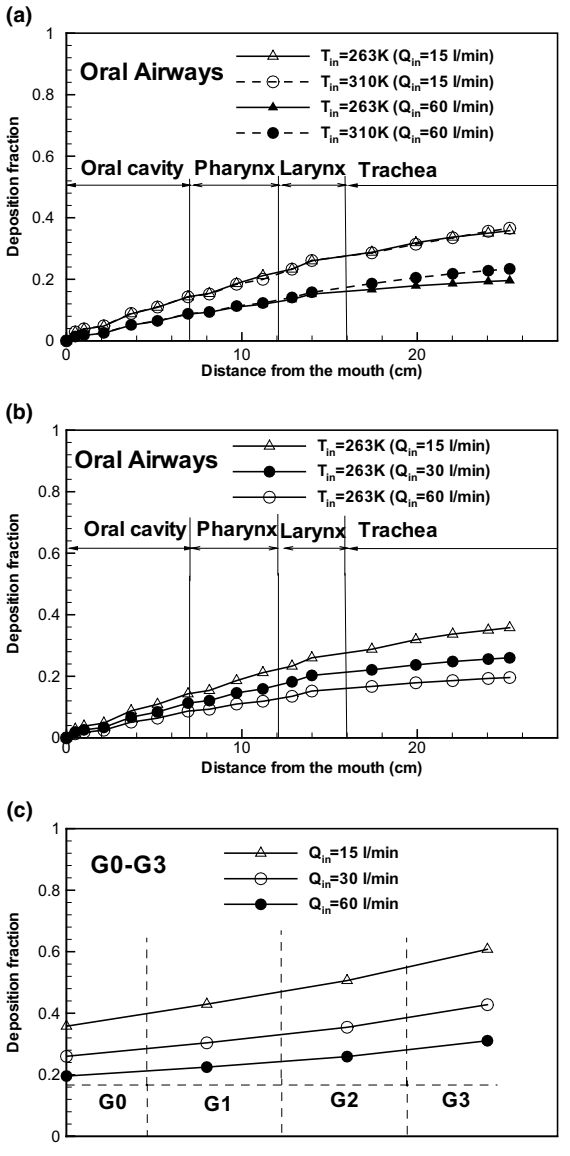

Fig. 8. Deposition fractions of JP-8 fuel vapor in the upper human airway.

residence times for vapors with low flow rates and is consistent with the experimental observations of Li et al. [8] for deposition of Iodine vapor in a tracheobronchial cast. The deposition fraction may increase 75–120% in the oral airways and G0–G3 when switching from exercise breathing ($Q_{in} = 60$ l/min) to low-level breathing ($Q_{in} = 15$ l/min). The deposition fraction of JP-8 fuel vapor in the oral airway and G0–G3 under resting condition can be as high as 36% and 25%, respectively. Of interest is that the curves of deposition fractions in the trachea for relatively high inspiratory flow rate cases are a little steeper than that for the low inspiratory flow rate case; this indicates the effect of turbulent dispersion on vapor deposition (Fig. 8a and b).

5.5. Calculation of heat transfer coefficient

The respiratory heat transfer coefficient (h_c) is a phenomenological constant relating the heat flux to the temperature difference between the "free" airstream and

the airway walls. The local h_c is difficult to determine in the junction area of bifurcation airways; hence, regional (i.e., segmental) h_c-values are calculated instead of the local h_c. In any segmental unit (e.g., oral airway, first, second or third bifurcation), the energy balance is

$$q''A_{\text{wall}} = \sum_{i=1}^{n} \dot{m}_i H_i - \dot{m}_0 H_0 \tag{16}$$

where A_{wall} is the total wall surface area of the airway unit. The subscripts "0" and "i" denote the properties at the inlet (parent) and the ith daughter tube of a selected airway unit, respectively. In the oral airway model, the "i" denotes the trachea and $n = 1$; $\dot{m}$ is the mass flow rate determined as

$$\dot{m} = \int_A u \, \mathrm{d}A \tag{17}$$

The regional heat transfer coefficient is calculated as

$$h_c = q''/(T_{\text{wall}} - T_m) \tag{18}$$

where T_m is the mean temperature of the "free" airstream in this region. In this paper, two approaches were considered to determine the mean temperature. For example, averaging the inlet and outlet cross-sectional mean bulk temperatures yields:

$$T_{m,1} = \frac{1}{2}\left[\frac{\int u_0 T_0 \, \mathrm{d}A_0}{\int u_0 \, \mathrm{d}A_0} + \frac{1}{n}\sum_{i=1}^{n} \frac{\int u_i T_i \, \mathrm{d}A_i}{\int u_i \, \mathrm{d}A_i}\right] \tag{19}$$

This simple approach was usually employed in experimental studies [15,16], where the cross-sectional mean bulk temperatures were replaced by the average values of locally measured temperatures at the inlet and outlets. Another approach to obtain T_m is based on the volumetric averaging of the bulk temperatures, i.e.

$$T_{m,2} = \frac{1}{\forall \cdot Q_0} \int_{\forall} V_{\text{speed}} \cdot T \, \mathrm{d}V \tag{20}$$

where $\forall$ is the volume of the airway unit, and Q_0, the inlet flow rate in this unit, and V_{speed}, the airstream speed.

Once the regional heat transfer coefficient is obtained, the region-averaged Nusselt number can be determined as

$$Nu = (h_c D)/\lambda \tag{21}$$

The diameters in the trachea and the parent tubes were used to calculate the Nu number for the oral airway and bifurcation units, respectively.

Fig. 9 shows the regional Nusselt number (Nu) in the oral airway model versus the product of the Reynolds (Re) and Prandtl (Pr) numbers as determined in the trachea based on the two different mean temperatures for the airstream. As expected, there are only small differences between the two calculated Nu numbers. Since $T_{m,1}$ is easier to compute for practical applications,

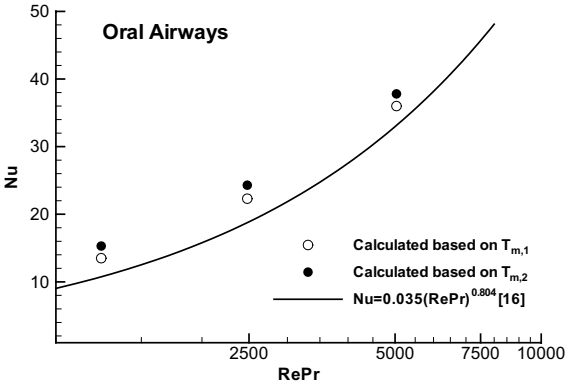

Fig. 9. Regional Nusselt number (Nu) versus the product of Re and Pr for human oral airways. The open and close circles represent the simulated Nu values while the line plots the values calculated from the correlation equation given by Nuckols [16].

Eq. (19) has been employed, unless otherwise noted. Compared with the empirical correlation obtained by Nuckols [16], the results generated by the computer simulation model almost match (Fig. 9). One cause for the discrepancy may be due to experimental uncertainties, e.g., cross-sectional averaging of non-uniform bulk temperatures cannot be obtained in the laboratory. Furthermore, two different oral airway geometries have been used in the present analysis and Nuckols' experiments [16].

Fig. 10a shows the regional Nu number as a function of $RePr$, as determined in the parent tube, for each individual bifurcation as well as for the entire bifurcation system of generations G0–G3. Of interest is that the regional Nu number is only a function of $RePr$, regardless of the specific bifurcation (e.g., the first, second or third bifurcation). However, the overall Nu-number distribution, i.e., for the entire three-bifurcation system, is somewhat higher than those for the individual bifurcations due to the non-homogenous flow and temperature distributions. The segmentally averaged convective heat transfer coefficient in dimensionless form for each bifurcation can be expressed as

$$Nu = 0.568(RePr)^{0.495} \quad 600 < Re < 6000 \tag{22}$$

where $r^2 = 0.99$, while for the entire triple bifurcation:

$$Nu = 0.66(RePr)^{1/2} \tag{23}$$

Comparison of the present correlation, Eq. (23), for the human upper bronchial tree with others [15,16] is given in Fig. 10b. Considering the slightly different model geometries (e.g., there is no smooth connection from the parent to the daughter tubes and the shape of the carinal ridge is sharp in their airway geometry [15,16]), as well as aforementioned experimental uncertainties, the present correlation agrees reasonably well with empirical data.

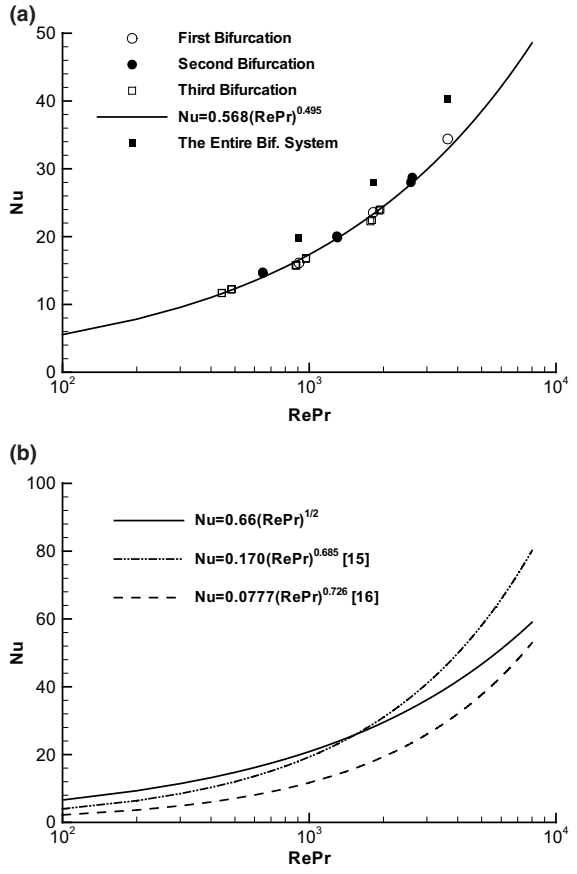

Fig. 10. Regional Nusselt number (*Nu*) versus the product of *Re* and *Pr* for human upper bronchial tree. The Nusselt numbers for the entire bifurcation system are the overall values over the total triple-bifurcation from G0 to G3.

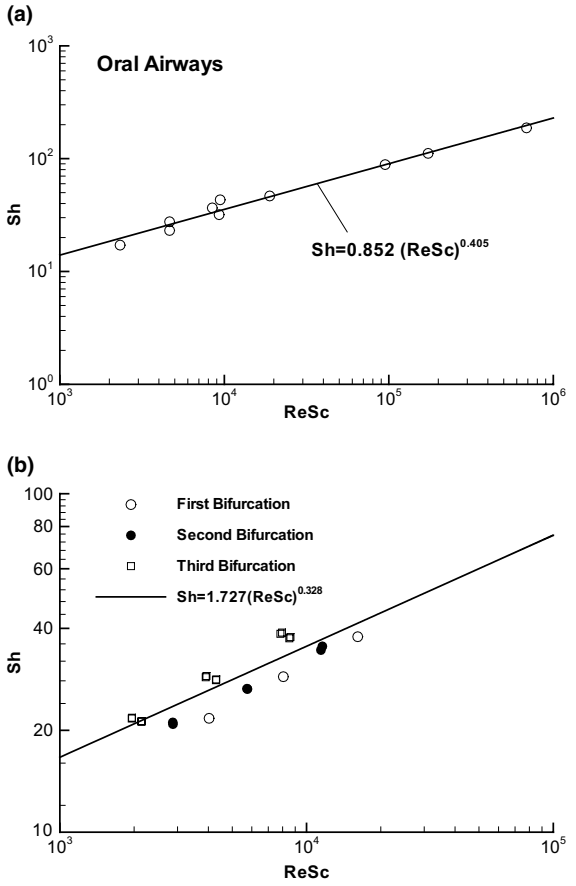

Fig. 11. Regional Sherwood number (*Sh*) versus the product of *Re* and *Sc* for: (a) human oral airways; and (b) human upper bronchial tree.

5.6. Calculation of mass transfer coefficient

Calculation of the respiratory mass transfer coefficient, h_m, is helpful in quantitatively predicting the regional uptake of inhaled ultrafine particles or vapors [4]. Similar to the calculation of h_c, the mass balance for one airway unit is

$$N \cdot A_{\text{wall}} = \sum_{i=1}^{n} \dot{m}_i Y_i - \dot{m}_0 Y_0 \tag{24}$$

which yields the wall mass flux of species N, so that

$$h_m = \frac{N}{\overline{\rho Y_m} - \rho Y_{\text{wall}}} \tag{25}$$

For simplicity, we only used the average values of the inlet and outlet cross-sectional mass fractions to determine the regional $\overline{\rho Y_m}$, i.e.,

$$\overline{\rho Y_m} = \frac{1}{2}\left[\frac{\int \rho_0 u_0 Y_0 \, dA_0}{\int \rho_0 u_0 \, dA_0} + \frac{1}{n}\sum_{i=1}^{n} \frac{\int \rho_i u_i Y_i \, dA_i}{\int \rho_i u_i \, dA_i}\right] \tag{26}$$

The Sherwood number (*Sh*), characteristic of convective dispersion, can be calculated as

$$Sh = (h_m D)/\widetilde{D} \tag{27}$$

Again, the diameters in the trachea and the parent tubes are employed to determine the *Sh* number for the oral airways and bifurcation units, respectively.

Fig. 11a depicts the regional Sherwood number (*Sh*) for the oral airway model versus the product of Reynolds (*Re*) and Schmidt (*Sc*) numbers, both evaluated in the trachea, based on different inhalation flow rates and diffusion coefficients (i.e., particle sizes). The correlation between *Sh* number and *ReSc* can be expressed as

$$Sh = 0.852(ReSc)^{0.405} \quad 1500 < Re < 7000, \quad 1 < Sc < 230 \tag{28}$$

where $r^2 = 0.99$. The convective mass transfer coefficients for JP-8 fuel vapor in terms of the *Sh* number has been also obtained for each individual bifurcation in

airway generations G0–G3 (Fig. 11b). Affected by the non-homogeneous airflow structures and mass concentration distributions, the regional *Sh* numbers are slightly different for each bifurcation. However, a best-fit correlation yielded (Fig. 11b):

$$Sh = 1.727(ReSc)^{0.328} \quad 600 < Re < 6000, \quad Sc \approx 3 \tag{29}$$

where $r^2 = 0.77$.

6. Conclusions

Employing a user-enhanced, experimentally validated computer simulation model, using the finite-volume code CFX as the solver [25], steady non-isothermal inhalation of fuel vapor or nano-size particles in the upper human airways have been analyzed and new Nusselt and Sherwood number correlations have been developed. The CFPD results show the following:

(1) Heat transfer effects in the oral airways are considerable at low-level breathing ($Q_{in} = 15$ l/min), where changing temperature distributions influence the velocity fields, especially in the trachea. However, the thermal impact tends to be negligible for medium to high-level breathing modes ($Q_{in} = 30$ to 60 l/min);
(2) Although the local vapor concentrations may be affected by non-isothermal flow, the total and segmental deposition fractions of (JP-8) fuel vapor in the upper airways are basically not influenced by variations in ambient temperature, i.e., $263 \leqslant T_{in} \leqslant 310$ K, where the variation of deposition fractions is within 15%.
(3) The flow rate has a significant effect on fuel vapor deposition, i.e., the higher the flow rate the lower is the deposition fraction; for example, the deposition fraction in the present system, i.e., mouth to Generation G3, changes from 30% to 60% when switching from high-level to low-level inhalation.
(4) The regional Nusselt number for the bronchial tree is the same for each bifurcation. However, the overall *Nu*-number distribution, i.e., averaged over the entire multi-bifurcation system, is somewhat higher than those for the individual bifurcations due to non-homogenous flow and temperature effects.

The methodology outlined and physical insight provided can be also applied to other complex intake configurations, such as engine ports and inlet ducts of air-breathing propulsion systems.

Disclaimer

The views and conclusions contained herein are those of the authors and should not be interpreted as necessarily representing the official policies or endorsements, either expressed or implied, of the Air Force Office of Scientific Research or the US Government.

Acknowledgements

This effort was sponsored by the Air Force Office of Scientific Research, Air Force Material Command, USAF, under grant number F49620-01-1-0492 (Dr. Walt Kozumbo, Program Manager) and the National Science Foundation (BES-0201271; Dr. Gil Devey, Program Director). The US Government is authorized to reproduce and distribute reprints for governmental purposes notwithstanding any copyright notation thereon. The use of CFX software from AEA Technology (Pittsburgh, PA) and access to the SGI Origin 2400 workstation at the North Carolina Supercomputing Center (Research Triangle Park, NC) are gratefully acknowledged as well.

References

[1] J.D. Pleil, L.B. Smith, S.D. Zelnick, Personal exposure to JP-8 jet fuel vapors and exhaust at air force bases, Environ. Health Perspec. 108 (2000) 183–192.
[2] H.E. Wichmann, A. Peters, Epidemiological evidence of the effects of ultrafine particle exposure, Phil. Trans. R. Soc. Lond. A. 358 (2000) 2751–2769.
[3] W.H. Finlay, The Mechanics of Inhaled Pharmaceutical Aerosols: An Introduction, Academic Press, London, UK, 2001.
[4] K.H. Cheng, Y.S. Cheng, H.C. Yeh, D.L. Swift, Measurements of airway dimensions and calculation of mass transfer characteristics of the human oral passage, J. Biomech. Eng.-Trans. ASME 119 (1997) 476–482.
[5] K.H. Cheng, Y.S. Cheng, H.C. Yeh, D.L. Swift, An experimental method for measuring aerosol deposition efficiency in the human oral airway, Am. Ind. Hyg. Assoc. J. 58 (3) (1997) 207–213.
[6] Y.S. Cheng, Y. Yamada, H.C. Yeh, D.L. Swift, Diffusional deposition of ultrafine aerosols in a human nasal cast, J. Aerosol Sci. 19 (1988) 741–751.
[7] B.S. Cohen, R.G. Sussman, M. Lippmann, Ultrafine particle deposition in a human tracheobronchial cast, Aerosol Sci. Technol. 12 (1990) 1082–1091.
[8] W. Li, J.Q. Xiong, B.S. Cohen, The deposition of unattached radon progeny in a tracheobronchial cast as measured with iodine vapor, Aerosol Sci. Technol. 28 (1998) 502–510.
[9] J.S. Kimbell, E.A. Gross, D.R. Joyner, M.N. Godo, K.T. Morgan, Application of computational fluid dynamics to regional dosimetry of inhaled chemicals in the upper respiratory tract of the rat, Toxicol. Appl. Pharmacol. 121 (1993) 253–263.
[10] G.M. Kepler, R.B. Richardson, K.T. Morgan, J.S. Kimbell, Computer simulation of inspiratory nasal airflow and

inhaled gas uptake in a rhesus monkey, Toxicol. Appl. Pharmacol. 150 (1998) 1–11.
[11] G. Yu, Z. Zhang, R. Lessmann, Computer simulation of the flow field and particle deposition by diffusion in a 3-D human airway bifurcation, Aerosol Sci. Technol. 25 (1996) 339–352.
[12] G. Yu, Z. Zhang, R. Lessmann, Fluid flow and particle diffusion in the human upper respiratory system, Aerosol Sci. Technol. 28 (1998) 146–158.
[13] C.S. Kim, Ultrafine particle deposition in a double bifurcation tube with human G3–G5 airway geometry, US EPA, Internal Report, 2002.
[14] Z. Zhang, C. Kleinstreuer, Low Reynolds number turbulent flows in locally constricted conduits: a comparison study, AIAA J. (2003) 831–840.
[15] C.E. Johnson, L.S. Linderoth Jr., M.L. Nuckols, An analysis of sensible respiratory heat exchange during inspiration under environmental condition of deep diving, J. Biomech. Eng.-Trans. ASME 99 (1977) 45–53.
[16] M.L. Nuckols, Heat and water transfer in the human respiratory system at hyperbaric conditions, PhD thesis, Duke University, Durham, NC, 1981.
[17] E.R. Weibel, Morphometry of the Human Lung, Academic Press, New York, 1963.
[18] E. Daviskas, I. Gonda, S.D. Anderson, Mathematical modeling of heat and water transport in human respiratory tract, J. Appl. Physiol. 69 (1) (1990) 362–372.
[19] L.M Hanna, P. Scherer, A theoretical model of localized heat and water transport in the human respiratory tract, J. Biomech. Eng. 108 (1986) 19–27.
[20] E.P. Ingenito, J. Solway, E.R. McFadden Jr., B.M. Pichurko, E.G. Cravalho, J.M. Drazen, Finite difference analysis of respiratory heat transfer, J. Appl. Physiol. 61 (6) (1986) 2252–2259.
[21] S. Naftali, R.C. Schroter, R.J. Shiner, D. Elad, Transport phenomena in the human nasal cavity: a computational model, Ann. Biomed. Eng. 26 (1998) 831–839.
[22] T. Martonen, Z. Zhang, Y. Yang, Particle diffusion from developing flows in rough-walled tubes, Aerosol Sci. Technol. 26 (1997) 1–11.
[23] D.C. Wilcox, Turbulence Modeling for CFD, DCW Industries, Inc., La Canada, CA, 1993.
[24] A. Bejan, Convection Heat Transfer, John Wiley & Sons, Inc., New York, 1995.
[25] AEA Technology, CFX-4.4: Solve, CFX International, Oxfordshire, UK, 2001.
[26] I.R. Morris, Functional anatomy of the upper airway, Emerg. Med. Clin. North Am. 6 (1988) 639–669.
[27] J.B. Gustafson, J.G. Tell, D. Orem, Selection of Representative TPH Fractions based on Fate and Transport Consideration, Amherst Scientific Publishers, Amherst, MA, 1997.
[28] B.J. Fan, Y.S. Cheng, H.C. Yeh, Gas collection efficiency and entrance flow effect of an annular diffusion denuder, Aerosol Sci. Technol. 25 (2) (1996) 113–120.
[29] J.K. Comer, C. Kleinstreuer, Z. Zhang, Flow structures and particle deposition patterns in double bifurcation airway models. Part 1. Air flow fields, J. Fluid Mech. 435 (2001) 25–54.
[30] Z. Zhang, C. Kleinstreuer, Transient airflow structures and particle transport in a sequentially branching lung airway model, Phys. Fluids 14 (2002) 862–880.
[31] C. Kleinstreuer, Z. Zhang, Laminar-to-turbulent fluid-particle flows in a human airway model, Int. J. Multiphase Flow (2003) 271–289.